Modeling of Surface Hairline-Crack Detection in Metals Under Coatings Using an Open-Ended Rectangular Waveguide

Christian Huber, *Member, IEEE,* H. Abiri, Stoyan I. Ganchev, *Senior Member, IEEE,* and R. Zoughi, *Senior Member, IEEE*

***Abstract*—A surface-breaking hairline crack or a narrow slot in a metallic specimen when scanned by an open-ended rectangular waveguide probe influences the reflection-coefficient properties of the incident dominant mode. Subsequent recording of a change in the standing-wave pattern while scanning such a surface results in what is known as the *crack characteristic signal*. Since microwave signals penetrate inside dielectric materials, this methodology is capable of detecting cracks under dielectric coatings of various electrical thicknesses as well. To electromagnetically model the interaction of an open-ended rectangular waveguide with a surface-breaking hairline crack under a dielectric coating, the dielectric-coating layer is modeled as a waveguide with a large cross section. Thus, the problem is reduced to a system of three waveguides interacting with each other while the location of the crack is continuously changing relative to the probing waveguide aperture (a dynamic scanning problem). An analysis of modeling the dielectric-coating layer as a dielectric-filled waveguide with a large cross section is given, and its comparison with radiation into an unbounded medium is presented. For obtaining the reflection coefficients of the dominant and higher order modes, the electromagnetic properties of the probing waveguide—dielectric-coating layer junction and the dielectric-coating layer—crack junction are separately analyzed. For each junction, a magnetic-current density M is introduced over the common aperture. Subsequently, the junction formed by the two respective waveguide sections is separated into two systems. A numerical solution employing the method of moments is obtained, and the properties of the junctions are expressed by their respective generalized scattering matrices. Consequently, the generalized scattering matrix for the total system can be evaluated. The convergence behavior of the system is studied to determine an optimal set of basis functions and the optimal number of higher order modes for a fast and accurate solution. Finally, the theoretical and measured *crack characteristic signals* are compared.**

***Index Terms*— Method of moments, microwave inspection, stress crack.**

Manuscript received April 3, 1997; revised July 18, 1997. This work was supported by the Federal Highway Administration under Contract DTFH61-94-X-00023.

C. Huber was with the Applied Microwave Nondestructive Testing Laboratory (AMNTL), Department of Electrical Engineering, Colorado State University, Ft. Collins, CO 80523 USA. He is now with Anaren Microwave, Inc., Syracuse, NY 13210 USA.

H. Abiri is with the Applied Microwave Nondestructive Testing Laboratory (AMNTL), Department of Electrical Engineering, Colorado State University, Ft. Collins, CO 80523 USA, on leave from the Electrical Engineering Department, Shiraz University, Shiraz, Iran.

S. I. Ganchev was with the Applied Microwave Nondestructive Testing Laboratory (AMNTL), Department of Electrical Engineering, Colorado State University, Ft. Collins, CO 80523 USA. He is now with Hewlett-Packard Company, Englewood, CO 80523-1373 USA.

R. Zoughi is with the Applied Microwave Nondestructive Testing Laboratory (AMNTL), Department of Electrical Engineering, Colorado State University, Ft. Collins, CO 80523 USA.

Publisher Item Identifier S 0018-9480(97)08023-X.

I. Introduction

METAL fatigue/cracking and subsequent failure results from environmentally accelerated fracture (i.e., corrosion accelerated) as well as large stress gradients. Examples of applications in which this type of metal failure may occur are aircraft fuselage, turbine blades, and steel-bridge members. Many such systems are operating even beyond their design lifetime which requires more than the originally prescribed inspection cycles. Cracks under coatings such as paint, rust, composite laminates, and corrosion protective substances are not always reliably detected using the conventional nondestructive evaluation (NDE) methods. The same applies to cracks filled with dielectric materials such as rust, dirt, paint, ice, and other foreign matters. Identification of the exact location of crack tips is another important practical issue (for prevention of crack propagation), which is not fully addressed by conventional NDE techniques. Environmental concerns must also be addressed when using an NDE technique (e.g., concerns associated with the dye-penetrant method). Removal of surface coating to facilitate crack detection is an undesirable procedure. Furthermore, remote crack detection (i.e., a standoff distance between the surface under test and the detection probe) is very desirable from a practical standpoint. In order to reduce the cost and increase testing efficiency and reliability, which subsequently improve the safety of metallic structures, it is necessary to develop a highly reliable, fast, and inexpensive NDE technique which will posses certain unique features. These features include detection of filled and covered cracks, remote detection, applicability to ferromagnetic and nonferromagnetic metals, environmental compliance, safety and ease of operation, portability, functionality in real-time and on-site, and easy adaptability to large area testing. There are many conventional nondestructive testing (NDT) methods used for interrogating metal surfaces; however, each method possesses certain limitations and disadvantages [1]. In some environments, the technique used may not be an optimum one, but the *only* one that can be applied.

In recent studies, an open-ended rectangular waveguide probe has been used to detect and size metal surface-breaking cracks [2]–[5]. This probe is capable of detecting surface cracks covered with dielectric coatings and/or filled with dielectric materials such as dirt, rust, or paint. Additionally, it is possible to locate crack tips, which is important in the light of preventing crack propagation [6]. A comprehensive discussion of the capabilities of this approach and the opti-

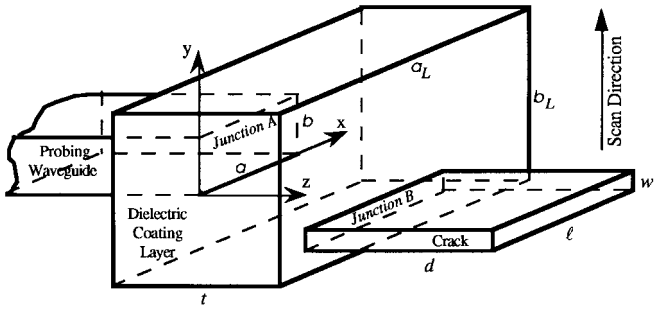

Fig. 1. Relative geometry of a surface crack, a dielectric-coating layer, and the waveguide aperture (not to scale).

mization possibilities for enhanced crack-detection sensitivity are presented in [7]. This paper presents a general model for electromagnetically describing the interaction of an open-ended rectangular waveguide with a *coated* surface-breaking hairline crack. A comparison between the numerical and the experimental results is also given.

II. System Description

The analysis of the electromagnetic properties of an open-ended rectangular waveguide radiating into a dielectric-coating layer, together with the interaction of the radiated field with a cracked metal surface, is a complicated analytical problem. In addition, this is a near-field problem, and no simplifying assumptions of plane waves can be made. From the formulation point of view, it is easier to treat the propagation of waves from a probing waveguide through a dielectric-coating layer onto a cracked metal surface as a system of three waveguides. The dielectric-coating layer is represented by an oversized waveguide (dimensions a_L and b_L) filled with the coating dielectric (for simulating remote detection it is filled with air), and the crack is represented by a short-circuited waveguide (dimensions w, ℓ, and d), as shown in Fig. 1. The dielectric-coating thickness represented by the length of the oversized waveguide section t is generally small (i.e., paint thickness). As will be seen later, the oversized waveguide representing the coating layer is a reasonable approximation of radiation into an unbounded medium.

A general representation of the system formed by the three waveguides is obtained by assuming arbitrary incident electric and magnetic fields in the probing waveguide. The incident and reflected fields in the waveguide, the dielectric-coating layer, and the crack are expressed in terms of their discrete orthonormal eigenfunctions with unknown complex coefficients. Applying the equivalence principle allows the system to be separated into three waveguide sections (two waveguide junctions) representing the probing waveguide, the dielectric-coating layer, and the crack [8]. The method of moments is then applied to obtain the solution for the complex field coefficients [9]. Subsequently, by arranging the system of equations in a matrix form and solving for the reflection coefficients at each of the two junctions, the generalized scattering matrices for the two junctions can be formulated [10]. Finally, the total generalized scattering matrix describing the overall system is derived by applying the transmission-line theory. The accuracy by which the electric- and magnetic-field distributions anywhere in the probing waveguide, the dielectric-coating layer, and in the crack are calculated depends on the number of higher order modes used and on the appropriate choice of basis functions. For analyzing these issues, the convergence behavior of the system is studied. Once the overall generalized scattering matrix is known, one point on the *crack characteristic signal* can be evaluated (i.e., a specific location of the crack relative to the probing waveguide aperture). *Crack characteristic signal* is referred to the detector voltage variations as a function of the scanning distance, when sensing the standing-wave voltage at a fixed location away from the aperture [2]. Hence, a *dynamic* numerical evaluation for obtaining the *crack characteristic signal* is performed.

III. Junction A: Probing Waveguide–Dielectric-Coating Layer

A. Field Components

The respective fields in the probing waveguide and the dielectric-coating layer represented by the oversized waveguide (see Fig. 1) are described by their orthonormal mode vectors which form complete sets [11]. By normalization, the power is divided between the modes according to the square of their amplitudes [12].

For a general case, it is assumed that all higher order TE and TM modes are generated at Junction A. Therefore, the total transverse electric and magnetic fields, expressed in terms of the orthonormal mode vectors of the probing waveguide (index a), are written as

$$\boldsymbol{E}_{at} = \sum_i C_i e^{-\gamma_{ai} z} \boldsymbol{e}_{ai} + \sum_i A_i e^{\gamma_{ai} z} \boldsymbol{e}_{ai} \tag{1a}$$

$$\boldsymbol{H}_{at} = \sum_i C_i Y_{ai} e^{-\gamma_{ai} z} \boldsymbol{u}_z \times \boldsymbol{e}_{ai} - \sum_i A_i Y_{ai} e^{\gamma_{ai} z} \boldsymbol{u}_z \times \boldsymbol{e}_{ai}. \tag{1b}$$

$\boldsymbol{u}_z$ denotes the unit vector in the direction of propagation, and $\{C_i\}$ and $\{A_i\}$ are complex coefficients of the incident and reflected modes, respectively. Similarly, in the dielectric-coating layer side, the transverse fields can be expanded in terms of the orthonormal modes (index c) as

$$\boldsymbol{E}_{ct} = \sum_i B_i e^{-\gamma_{ci} z} \boldsymbol{e}_{ci} - \sum_i E_i e^{\gamma_{ci} z} \boldsymbol{e}_{ci} \tag{2a}$$

$$\boldsymbol{H}_{ct} = \sum_i B_i Y_{ci} e^{-\gamma_{ci} z} \boldsymbol{u}_z \times \boldsymbol{e}_{ci} + \sum_i E_i Y_{ci} e^{\gamma_{ci} z} \boldsymbol{u}_z \times \boldsymbol{e}_{ci} \tag{2b}$$

where $\{B_i\}$ and $\{E_i\}$ are the complex coefficients of the forward and backward propagating modes in the dielectric-coating layer, respectively. The propagation constant for the probing waveguide and the dielectric-coating layer $\{\gamma_{qi}\}, q \in \{a, c\}$ are given by

$$\gamma_{qi} = \begin{cases} j\beta_i = jk_o \sqrt{1 - \left(\dfrac{\lambda_o}{\lambda_{qi}}\right)^2}, & \lambda_{qi} > \lambda_o \\ \beta_i = k_{qi} \sqrt{1 - \left(\dfrac{\lambda_{qi}}{\lambda_o}\right)^2}, & \lambda_o > \lambda_{qi} \end{cases} \tag{3}$$

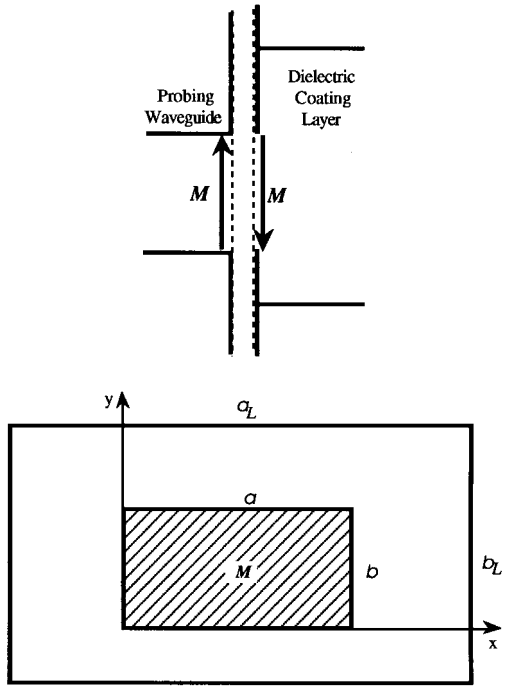

Fig. 2. The equivalent situation for the waveguide and the dielectric-coating layer.

where k_o is the wavenumber of the medium filling the respective waveguide, $\{k_{qi}\}$ is the mode cutoff wavenumber, while λ_o and $\{\lambda_{qi}\}$ are the corresponding wavelengths. The modal characteristic admittance $\{Y_{qi}\}$ in the waveguide and in the dielectric-coating layer is defined as

$$Y_{qi} = \begin{cases} \dfrac{\gamma_{qi}}{j\omega\mu_o} & \text{(TE modes)} \\ \dfrac{j\omega\varepsilon_o}{\gamma_{qi}} & \text{(TM modes).} \end{cases} \tag{4}$$

Forcing the boundary conditions for the transverse fields at Junction A allows solving for all the unknown field coefficients.

B. Formulating the Generalized Scattering Matrix

The system formed by the probing waveguide and the dielectric-coating layer (i.e., an oversized waveguide) is divided into two parts using the equivalence principle. According to the equivalence principle, the field in the probing waveguide is identical to the exciting field plus the field produced by an equivalent magnetic-current density $\boldsymbol{M}$, when the aperture S is replaced by a perfect conductor [8]. $\boldsymbol{M}$ is defined over the aperture S as

$$\boldsymbol{M} = \boldsymbol{u}_z \times \boldsymbol{E}_t|_{z=0}. \tag{5}$$

In the dielectric-coating layer, the total field is represented by a component which is a result of the reflection from the termination with a crack in a metal plate, plus the field produced by the equivalent magnetic-current density $-\boldsymbol{M}$ over the aperture S (as shown in Fig. 2). Hence, the total transverse electric and magnetic fields in the waveguide equivalent to (1) is now given by

$$\boldsymbol{E}_{at} = \sum_i C_i e^{-\gamma_{ai}z}\boldsymbol{e}_{ai} - \sum_i C_i e^{\gamma_{ai}z}\boldsymbol{e}_{ai} + \sum_i D_i e^{\gamma_{ai}z}\boldsymbol{e}_{ai} \tag{6a}$$

$$\boldsymbol{H}_{at} = \sum_i C_i Y_{ai} e^{-\gamma_{ai}z}\boldsymbol{u}_z \times \boldsymbol{e}_{ai} + \sum_i C_i Y_{ai} e^{\gamma_{ai}z}\boldsymbol{u}_z \times \boldsymbol{e}_{ai} - \sum_i D_i Y_{ai} e^{\gamma_{ai}z}\boldsymbol{u}_z \times \boldsymbol{e}_{ai}. \tag{6b}$$

Here, $\{C_i\}$ and $\{D_i\}$ are the respective coefficients of the incident modes and the modes produced by $\boldsymbol{M}$. In the dielectric-coating layer, the total transverse fields equivalent to (2) are then given by

$$\boldsymbol{E}_{ct} = \sum_i E_i e^{-\gamma_{ci}z}\boldsymbol{e}_{ci} - \sum_i E_i e^{\gamma_{ci}z}\boldsymbol{e}_{ci} + \sum_i F_i e^{-\gamma_{ci}z}\boldsymbol{e}_{ci} \tag{7a}$$

$$\boldsymbol{H}_{ct} = \sum_i E_i Y_{ci} e^{-\gamma_{ci}z}\boldsymbol{u}_z \times \boldsymbol{e}_{ci} + \sum_i E_i Y_{ci} e^{\gamma_{ci}z}\boldsymbol{u}_z \times \boldsymbol{e}_{ci} + \sum_i F_i Y_{ci} e^{-\gamma_{ci}z}\boldsymbol{u}_z \times \boldsymbol{e}_{ci} \tag{7b}$$

with $\{E_i\}$ and $\{F_i\}$ as the respective coefficients of the reflected modes and the modes produced by $-\boldsymbol{M}$. The last term in each of the above transverse fields (6) and (7) corresponds to the fields generated by the equivalent magnetic-current density $\boldsymbol{M}$ (i.e., at $z = 0$ the first two terms cancel each other).

At Junction A, the tangential electric-field components must vanish over all conducting surfaces (Area 1). Both the tangential components of the electric and magnetic fields must be continuous over the common aperture S (Area 2). The continuity of the transverse electric field $\boldsymbol{E}_t$ across the common aperture S is satisfied by the placement of an equivalent magnetic-current density $\boldsymbol{M}$. This equivalent magnetic-current density can be evaluated from (5) to (7) as

$$\boldsymbol{M} = \boldsymbol{u}_z \times \boldsymbol{E}_{at}|_{z=0} = \sum_i D_i \boldsymbol{u}_z \times \boldsymbol{e}_{ai} \tag{8a}$$

and

$$\boldsymbol{M} = \boldsymbol{u}_z \times \boldsymbol{E}_{ct}|_{z=0} = \sum_i F_i \boldsymbol{u}_z \times \boldsymbol{e}_{ci}. \tag{8b}$$

Similarly, the continuity of $\boldsymbol{H}_t$ across the aperture S requires that

$$2\sum_i C_i Y_{ai}\boldsymbol{u}_z \times e_{ai} - \sum_t D_i Y_{ai}\boldsymbol{u}_z \times \boldsymbol{e}_{ai} = 2\sum_i E_i Y_{ci}\boldsymbol{u}_z \times \boldsymbol{e}_{ci} + \sum_i F_i Y_{ci}\boldsymbol{u}_z \times \boldsymbol{e}_{ci}. \tag{9}$$

Subsequently, a numerical solution to (9) is obtained using the method of moments [9]. The equivalent magnetic-current density $\boldsymbol{M}$ is expanded as a complete set of N real valued basis functions $\{\boldsymbol{M}_j\}$:

$$\boldsymbol{M} = \sum_{j=1}^{N} V_j \boldsymbol{M}_j \tag{10}$$

where $\{V_j\}$ are unknown complex coefficients. The number of modes is chosen to be L_a in the probing waveguide and L_c in

the dielectric-coating layer. Now, by substituting for $\boldsymbol{M}$ from (8a) and (8b) using orthogonality of mode vectors, and by scalarly multiplying by $\boldsymbol{u}_z \times \boldsymbol{e}_{ak}$ and $\boldsymbol{u}_z \times \boldsymbol{e}_{ck}$, respectively, and then integrating over the corresponding waveguide and dielectric-coating apertures S_a and S_c, the following equations are obtained:

$$D_i = \sum_{j=1}^{N} V_j H_{aij}, \qquad i = 1, 2, \cdots, L_a \tag{11a}$$

$$F_i = \left(\sum_{j=1}^{N} V_j H_{cij} \right), \qquad i = 1, 2, \cdots, L_c \tag{11b}$$

where

$$H_{aij} = \iint_{S_a} \boldsymbol{M}_j \cdot \boldsymbol{u}_z \times \boldsymbol{e}_{ai}\, dS_a \tag{12a}$$

$$H_{cij} = \iint_{S_c} \boldsymbol{M}_j \cdot \boldsymbol{u}_z \times \boldsymbol{e}_{ci}\, dS_c. \tag{12b}$$

In order to evaluate the unknown coefficients in (9), Galerkin's method is applied, and after substitution for D_i and F_i from (11), the following is obtained:

$$\begin{aligned} 2\sum_{i=1}^{L_a} C_i Y_{ai} P_{aik} - 2\sum_{i=1}^{L_c} E_i Y_{ci} P_{cik} \\ = \sum_{i=1}^{L_a} \left(\sum_{j=1}^{N} V_j H_{aij} \right) Y_{ai} P_{aik} \\ + \sum_{i=1}^{L_c} \left(\sum_{j=1}^{N} V_j H_{cij} \right) Y_{ci} P_{cik} \end{aligned} \tag{13}$$

where

$$P_{aik} = \iint_{S_a} \boldsymbol{M}_k \cdot \boldsymbol{u}_z \times \boldsymbol{e}_{ai}\, dS_a \tag{14a}$$

$$P_{cik} = \iint_{S_c} \boldsymbol{M}_k \cdot \boldsymbol{u}_z \times \boldsymbol{e}_{ci}\, dS_c. \tag{14b}$$

With a matrix representation it is possible to write

$$\vec{C} = [C_i]_{L_a \times 1} \tag{15}$$

$$\vec{D} = [D_i]_{L_a \times 1} = [H_{aij}][V_j] = \boldsymbol{H}_a \vec{V} \tag{16}$$

$$\vec{E} = [E_i]_{L_c \times 1} \tag{17}$$

$$\vec{F} = [F_i]_{L_c \times 1} = [H_{cij}][V_j] = \boldsymbol{H}_c \vec{V}. \tag{18}$$

The set of (13) is now written in a matrix form as

$$\vec{I} = [\overline{\boldsymbol{Y}}_a + \overline{\boldsymbol{Y}}_c]\vec{V} \tag{19}$$

where

$$\vec{I} = 2\boldsymbol{P}_a^T \boldsymbol{Y}_a \vec{C} - 2\boldsymbol{P}_c^T \boldsymbol{Y}_c \vec{E} \tag{20a}$$

$$\overline{\boldsymbol{Y}}_a = \boldsymbol{P}_a^T \boldsymbol{Y}_a \boldsymbol{H}_a \tag{20b}$$

$$\overline{\boldsymbol{Y}}_c = \boldsymbol{P}_c^T \boldsymbol{Y}_c \boldsymbol{H}_c. \tag{20c}$$

$\boldsymbol{Y}_a$ and $\boldsymbol{Y}_c$ are diagonal matrices whose elements are evaluated as

$$\boldsymbol{Y}_a = [Y_{ai}]_{L_a \times L_a} \tag{21a}$$

$$\boldsymbol{Y}_c = [Y_{ci}]_{L_c \times L_c}. \tag{21b}$$

Note that $\boldsymbol{P}_a^T = \boldsymbol{H}_a^T$ and $\boldsymbol{P}_c^T = \boldsymbol{H}_c^T$ when using the Galerkin's method.

Now it is possible to evaluate the generalized scattering matrix $\boldsymbol{S}^A$ of Junction A, which is described by

$$\boldsymbol{S}^A = \begin{bmatrix} \boldsymbol{S}_{11}^A & \boldsymbol{S}_{12}^A \\ \boldsymbol{S}_{21}^A & \boldsymbol{S}_{22}^A \end{bmatrix}. \tag{22}$$

Let $\{A_i\}$ be the coefficient vector of the reflected modes in the probing waveguide given by

$$\vec{A} = [A_i]_{L_a \times 1} \tag{23a}$$

and let $\{B_i\}$ be the coefficient vector of the reflected modes in the dielectric-coating layer given by

$$\vec{B} = [B_i]_{L_c \times 1}. \tag{23b}$$

From (1), (2), (6), and (7) the reflected waves are given by

$$\vec{A} = \vec{D} - \vec{C} \tag{24a}$$

$$\vec{B} = \vec{E} + \vec{F}. \tag{24b}$$

Evaluating $\vec{V}$ from (19) and (20) gives

$$\vec{V} = 2[\overline{\boldsymbol{Y}}_a + \overline{\boldsymbol{Y}}_b]^{-1}[\boldsymbol{P}_a^T \boldsymbol{Y}_a \vec{C} - \boldsymbol{P}_c^T \boldsymbol{Y}_c \vec{E}]. \tag{25}$$

Substituting for $\vec{D}$ and $\vec{F}$ from (16) and (18) evaluates to

$$\vec{D} = \boldsymbol{H}_a \vec{V} = \boldsymbol{H}_a 2[\overline{\boldsymbol{Y}}_a + \overline{\boldsymbol{Y}}_b]^{-1}[\boldsymbol{P}_a^T \boldsymbol{Y}_a \vec{C} - \boldsymbol{P}_c^T \boldsymbol{Y}_c \vec{E}] \tag{26a}$$

$$\vec{F} = \boldsymbol{H}_c \vec{V} = \boldsymbol{H}_c 2[\overline{\boldsymbol{Y}}_a + \overline{\boldsymbol{Y}}_b]^{-1}[\boldsymbol{P}_a^T \boldsymbol{Y}_a \vec{C} - \boldsymbol{P}_c^T \boldsymbol{Y}_c \vec{E}]. \tag{26b}$$

Now, in order to obtain $\boldsymbol{S}_{11}^A$ and $\boldsymbol{S}_{21}^A$, $\vec{E}$ is set to zero, and subsequently after substitution of (26), $\boldsymbol{S}_{11}^A$ and $\boldsymbol{S}_{21}^A$ are expressed as

$$\boldsymbol{S}_{11}^A = \vec{A}\vec{C}^{-1}|_{\vec{E}=0} = 2\boldsymbol{H}_a[\overline{\boldsymbol{Y}}_a + \overline{\boldsymbol{Y}}_c]^{-1}\boldsymbol{P}_a^T \boldsymbol{Y}_a - \boldsymbol{U} \tag{27}$$

$$\boldsymbol{S}_{21}^A = \vec{B}\vec{C}^{-1}|_{\vec{E}=0} = 2\boldsymbol{H}_c[\overline{\boldsymbol{Y}}_a + \overline{\boldsymbol{Y}}_c]^{-1}\boldsymbol{P}_a^T \boldsymbol{Y}_a \tag{28}$$

where $\boldsymbol{U}$ is the unity matrix. From (24) and (26), it follows that with $\vec{C}$ being zero for evaluating $\boldsymbol{S}_{12}^A$ and $\boldsymbol{S}_{22}^A$, these submatrices are given by

$$\boldsymbol{S}_{12}^A = -\vec{A}\vec{E}^{-1}|_{\vec{C}=0} = 2\boldsymbol{H}_a[\overline{\boldsymbol{Y}}_a + \overline{\boldsymbol{Y}}_c]^{-1}\boldsymbol{P}_c^T \boldsymbol{Y}_c \tag{29}$$

$$\boldsymbol{S}_{22}^A = -\vec{B}\vec{E}^{-1}|_{\vec{C}=0} = 2\boldsymbol{H}_c[\overline{\boldsymbol{Y}}_a + \overline{\boldsymbol{Y}}_c]^{-1}\boldsymbol{P}_c^T \boldsymbol{Y}_c - \boldsymbol{U}. \tag{30}$$

Note that S_{ij}^A is the amplitude of the ith mode due to the jth incident mode of unit amplitude.

TABLE I
COMPARISON BETWEEN RADIATING INTO AN INFINITE HALF-SPACE AND A LARGE WAVEGUIDE SECTION

Dielectric Constant	Radiation into infinite half-space by Lewin, and by Ganchev et al.	Radiation into larger waveguide section representing the dielectric layer	% Error in $\|\Gamma\|$	% Error in φ
Air $\varepsilon_r = 1.0 - j0.0$	$\|\Gamma\|$=0.256, φ=-82.18°	$\|\Gamma\|$=0.285, φ=-60.44°	11.33	26.45
Paint $\varepsilon_r = 3.0 - j0.2$	$\|\Gamma\|$=0.384, φ=-168.83°	$\|\Gamma\|$=0.385, φ=-154.23°	0.26	8.65
Carbon Black Loaded Composite $\varepsilon_r = 12.0 - j3.0$	$\|\Gamma\|$=0.615, φ=-178.78°	$\|\Gamma\|$=0.617, φ=-170.72°	0.33	4.51

C. Representation of the Dielectric-Coating Layer as a Waveguide Section

The dimensions of the waveguide section representing the dielectric-coating layer have to be sufficiently larger than those of the probing waveguide to approximate an infinite (in the transverse directions) dielectric-coating layer [13]. To check for the validity of this approximation, the reflection coefficient at the probing waveguide aperture is evaluated at a frequency of 24 GHz. The larger waveguide section is filled with different dielectrics such as air (simulating a lift-off or remote detection), paint, and a carbon-black loaded-dielectric composite. The results are compared with those for a waveguide radiating into an infinite half-space of the same dielectrics, as obtained by Lewin and by Ganchev *et al*. (see Table I) [14], [15]. It can be seen that for a lossless dielectric (air) the relative difference in the reflection coefficient (both its magnitude, $|\Gamma|$ and phase φ) of the dominant mode is relatively large. However, for lossy dielectrics the difference is smaller. Hence, the assumption of modeling the dielectric-coating layer as a waveguide with large cross section is deemed valid, and the total system formed by the probing waveguide, the dielectric-coating layer, and the crack can now be evaluated.

A closer approximation of radiating into an infinite half-space could be achieved by choosing larger dimensions for the waveguide section representing the dielectric-coating layer. However, the number of modes in the dielectric-coating layer then has to be increased to reach convergence (as will be seen later). The computer resources for the results shown here are a Pentium-based PC with 64 Mbytes of RAM. The results of Table I also indicate that the theoretical results for low-loss dielectric-coating layers, and when using remote detection, will somewhat deviate from the measurement results.

IV. JUNCTION B: DIELECTRIC-COATING LAYER CRACK

The evaluation of the generalized scattering matrix for Junction B, formed by the dielectric-coating layer and the crack, is identical to the one for the exposed crack [16]. Here, the dielectric-coating layer, represented as an oversized waveguide section, is the waveguide producing the fields incident on the crack. Due to the physical dimensions of the dielectric-coating layer, its TE_{10} mode, as well as other higher order modes, are propagating modes. Additionally, for the thickness of the dielectric-coating layer being very small, other higher order evanescent modes will be incident on the crack aperture. However, the formulation of the generalized scattering matrix as derived for Junction A can be applied in a similar fashion for Junction B. Hence, when taking the proper dimensions into account, it is possible to write the generalized scattering matrix for Junction B in matrix form as

$$\boldsymbol{S}_{11}^{B} = 2\boldsymbol{H}_c[\overline{\boldsymbol{Y}}_c + \overline{\boldsymbol{Y}}_b]^{-1}\boldsymbol{P}_c^{T}\boldsymbol{Y}_c - \boldsymbol{U}. \tag{31}$$

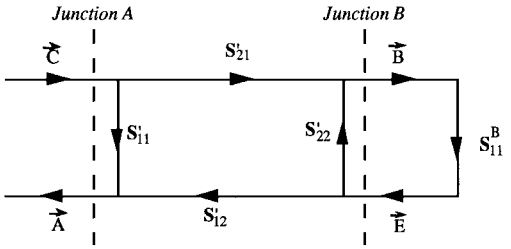

Fig. 3. Signal-flow graph of a system formed by a waveguide, a dielectric-coating layer, and a surface crack, represented in terms of its generalized scattering matrices.

V. THE TOTAL SYSTEM

When bringing the two individually derived generalized scattering matrices for Junctions A and B together, the output port of Junction A is shifted by the thickness of the dielectric-coating layer t. Hence, the generalized scattering matrix for Junction A is transformed to

$$\boldsymbol{S}' = \boldsymbol{T}\boldsymbol{S}^{A}\boldsymbol{T} \tag{32}$$

where $\boldsymbol{T}$ is a diagonal matrix with diagonal submatrices. Each submatrix represents the shift of the reference plane for that port. As the input port is not shifted, that submatrix is the identity matrix. The diagonal elements of output-port submatrix are calculated as

$$\boldsymbol{T}' = [e^{-\gamma_{ci}t}]|_{L_c \times L_c}, \tag{33}$$

Hence, $\boldsymbol{T}$ can be written as

$$\boldsymbol{T} = \begin{bmatrix} \boldsymbol{I} & 0 \\ 0 & \boldsymbol{T}' \end{bmatrix}. \tag{34}$$

Therefore, it readily follows that the elements of the generalized scattering matrix $\boldsymbol{S}'$ are evaluated as

$$\boldsymbol{S}'_{11} = \boldsymbol{S}^{A}_{11} \tag{35}$$
$$\boldsymbol{S}'_{12} = \boldsymbol{S}^{A}_{12}\boldsymbol{T}' \tag{36}$$
$$\boldsymbol{S}'_{21} = \boldsymbol{T}'\boldsymbol{S}^{A}_{21} \tag{37}$$
$$\boldsymbol{S}'_{22} = \boldsymbol{T}'\boldsymbol{S}^{A}_{22}\boldsymbol{T}'. \tag{38}$$

The signal-flow graph of the combined junctions, where Junction A and the dielectric-coating layer are represented as a two-port device, and Junction B and the crack are represented as a one-port device, is shown in Fig. 3. It immediately follows that the total generalized scattering matrix for the system can be evaluated as

$$\boldsymbol{S}^{\text{tot}}_{11} = \boldsymbol{S}'_{11} + \boldsymbol{S}'_{12}[\boldsymbol{U} - \boldsymbol{S}'_{22}\boldsymbol{S}^{B}_{11}]^{-1}\boldsymbol{S}^{B}_{11}\boldsymbol{S}'_{21}. \tag{39}$$

In order to calculate the *crack characteristic signal* for covered cracks, it is necessary to evaluate the generalized scattering matrix $\boldsymbol{S}^{\text{tot}}_{11}$ (reflection coefficient of the dominant mode and each of the higher order modes) for different positions of the crack relative to the waveguide aperture. Once the reflection coefficient of the incident dominant TE_{10} mode is known, the shift in the standing wave in the probing waveguide can be evaluated. Subsequently, the detector diode

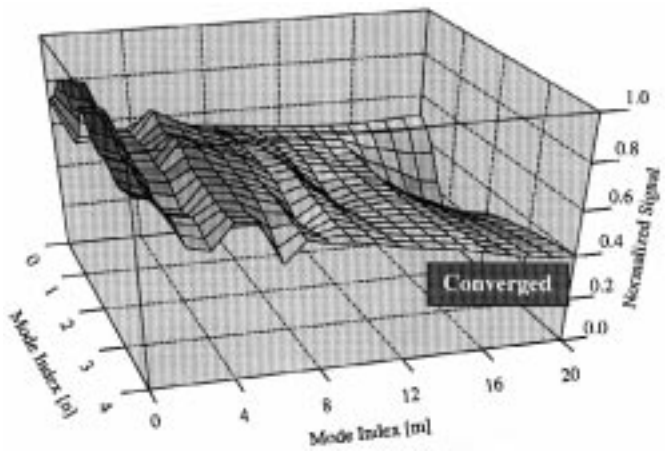

Fig. 4. Convergence plane for a long crack with a width of 0.84 mm and a depth of 1.53 mm, covered with a 1-mm-thick dielectric, such as paint ($\varepsilon_r = 3.0 - j0.2$), at the relative coordinates ($x = 0$ mm, $y = -0.8$ mm).

output voltage (probing the standing wave in the probing waveguide) for the dominant mode detection technique can be computed to obtain the *crack characteristic signal* [2].

VI. Convergence

The convergence behavior of this moment-solution approach is fully investigated and described in [16]. The first step is to choose a complete set of basis functions describing the initially unknown equivalent magnetic-current density $\boldsymbol{M}$. In order to obtain a relatively fast convergence, the basis functions for the two junctions are chosen to be similar to the orthonormal mode vectors of the transverse magnetic fields. For fast convergence, the number of basis functions should be optimally chosen. Since the aperture opening of the two junctions is not changing (the cross section of the waveguide and the crack), the number of the basis functions may be kept relatively small. The following practical criteria has been established for the appropriate maximal number of basis functions in x-direction: q' and p', and y-direction: q and p:

$$q'_{\max} = p'_{\max} = q_{\max} = p_{\max} = \begin{cases} 2, & t \geq 1 \text{ mm} \\ \operatorname{ceil}\left(2 + \ln\left(\frac{1}{t}\right)\right), & t < 1 \text{ mm}. \end{cases} \quad (40)$$

The operator (ceil) means rounding off to the larger integer. For low-loss dielectrics, this number should be increased further.

The next step is to obtain a criteria for the optimal number of modes in the probing waveguide, the dielectric-coating layer, and the crack. This number depends on the dimensions of the three transmission lines and the dielectric properties of the coating layer. For the probing waveguide and the crack, the number of modes is the same as the number of basis functions. All of the modes up to these indexes should be considered, and degenerate modes should be included separately [17]. To find the optimal number of modes in the dielectric-coating layer, the typical convergence behavior is studied for an increasing number of modes. The result for a crack/slot with a width of 0.84 mm and a depth of 1.53 mm at the relative coordinates ($x = 0$ mm, $y = -0.8$ mm) is given in Fig. 4. The crack is covered with a 1-mm-thick dielectric-coating layer with $\varepsilon_r = 3.0 - j0.2$ (similar to the dielectric constant of common paint). The results indicate that a relatively small number of modes (80) are needed to reach convergence when the crack is at the edge (i.e., the crack just entering the waveguide aperture). For the exposed crack, over 200 modes were necessary for this geometry [16]. The significant reduction in the number of modes necessary for the calculations is due to the already mentioned fact that for both Junctions A and B, the waveguide and the crack apertures are fully within the aperture of the dielectric-coating layer. A study of the convergence behavior for the crack at different relative positions with respect to the waveguide aperture has shown that the maximal indexes $n_{c,\max}$ and $m_{c,\max}$ of the desired number of TE_{nm} and TM_{nm} modes in the dielectric-coating layer are given by

$$n_{c,\max} = \max\left\{\operatorname{ceil}\left(\frac{q_{\max} a_L}{a}\right), \operatorname{ceil}\left(\frac{q_{\max} a_L}{\ell}\right)\right\} \quad (41a)$$

$$m_{c,\max} = \max\left\{\operatorname{ceil}\left(\frac{p_{\max} b_L}{b}\right), \operatorname{ceil}\left(\frac{p_{\max} b_L}{w}\right)\right\}. \quad (41b)$$

The operator (max) means taking the larger of the two integers. It has to be noted that the number of modes in the dielectric-coating layer has to be chosen equal for the two separate evaluations of Junction A and Junction B, as the system is combined in the final step of evaluating $\boldsymbol{S}_{11}^{\mathrm{tot}}$.

VII. Results

As explained earlier, an important advantage of this microwave methodology is evident when it is used for detecting surface cracks under dielectric coatings. It must be noted that dielectric coatings such as paint and corrosion preventative substances may have various thicknesses, although they are generally not very thick. Therefore, it is important to establish the potentials and limitations of this microwave approach as a function of the electrical thickness of the dielectric coating covering a crack. In this section, the theoretical and experimental results (at a frequency of 24 GHz) on slots/cracks covered with thin sheets of wrapping paper are discussed. Wrapping paper has similar dielectric properties as common paint. Furthermore, wrapping paper (with uniform thickness of 0.04 mm) may easily be stacked on top of each other to provide for various thicknesses.

A. Covered Crack Detection and Comparison with Exposed Cracks

A slot with a width of 0.51 mm and a depth of 2 mm was covered with four (0.16 mm) and 24 (0.96 mm) sheets of wrapping paper, respectively, and its *crack characteristic signal* was calculated and measured at a frequency of 24 GHz (Fig. 5). For comparison purposes, the *crack characteristic signal* for the exposed crack (i.e., flush) is also presented. There are several features concerning the results which are worth mentioning. With a dielectric coating, the overall level of the recorded signal decreases compared to the exposed case. This is primarily due to the fact that the standing-wave pattern inside the waveguide is different when it is terminated by a

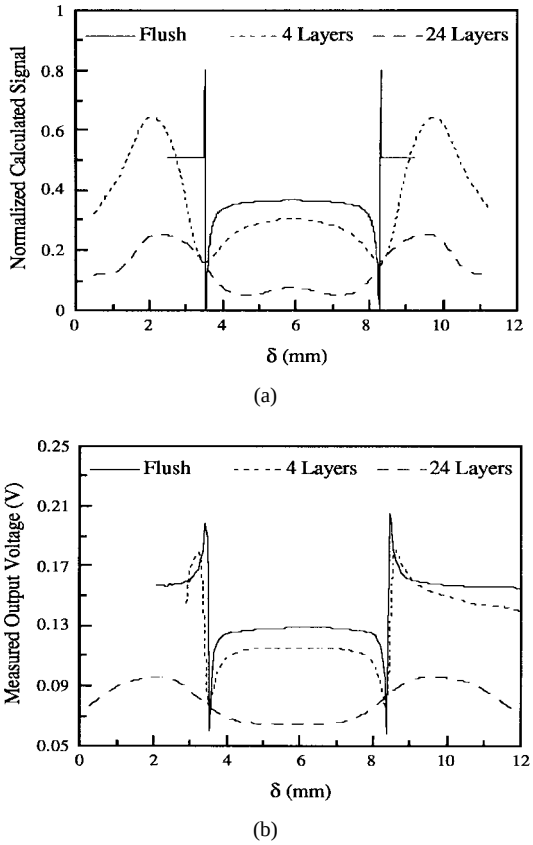

Fig. 5. Crack characteristic signals for a crack with a width of 0.51 mm and a depth of 2 mm at flush, and covered with four and 24 layers of wrapping paper (coating thickness of 0.16 and 1 mm, respectively) at a frequency of 24 GHz. (a) Calculated. (b) Measured.

conductor (i.e., flush) and when it is terminated by a dielectric covered conductor. Hence, the dynamic range of the *crack characteristic signal* decreases as shown. Furthermore, there will be a shift in the standing-wave pattern (compared to the case with no coating, i.e., flush) which in turn puts the fixed diode location at a different position on the standing-wave pattern. The incident signal is also attenuated by the two-way travel in the coating (although this attenuation may be small), contributing to a decreased signal level when detecting covered cracks. When the crack/slot is covered with 24 sheets (0.96 mm) of the wrapping paper, the dynamic range of the detected voltage for this *crack characteristic signal* is still large enough, indicating that many more layers of wrapping paper may cover this crack, and it will still be detectable. Coating thicknesses of greater than a couple of millimeters is considered unusually thick for paint and corrosion preventative substances. Thus, the results indicate the cracks under such thick coatings may be detected using this microwave method. Furthermore, the distance between the two sharp transitions increases due to the dielectric coating (Fig. 5). This is due to the fact that the incident microwave signal is able to interact with the crack edges (i.e., the aperture *sees* the crack edge) before it comes over it, unlike the flush case. Furthermore, the sharpness associated with the transitions degrades as a result of the dielectric coating. This is an important feature associated with covered cracks. This means, in practice, one may not need a fine resolution scanner for detecting covered cracks, since the possibility of jumping over the transitions in the *crack characteristic signal* is low, particularly for cracks whose depth is such that the middle-signal level and the signal level when the crack is outside the aperture are similar. Even for exposed cracks, it may be advantageous to use a dielectric coating in front of the waveguide aperture to decrease the possibility of missing the sharp transitions in the *crack characteristic signal*.

As the thickness of the coating increases, the *crack characteristic signal* shows less variation in its overall shape, making the detection of the crack more difficult. This is also true as the loss factor of the dielectric coating increases. Since the standing wave inside the waveguide is formed as a result of the interference between the reflected wave and the incident wave, it is reasonable to assume that an increase in the incident signal power will increase the reflected signal power. Consequently, cracks covered with thicker coatings have been detected [7].

B. Remote Crack Detection (Lift-off)

Lift-off (standoff distance) between the waveguide aperture and the surface of a specimen is an important practical parameter. Remote crack detection requires incorporating a lift-off between the waveguide probe and the surface under examination. Lift-off could be viewed in three ways:

1) finite thickness of air which may be present in most measurements or may be required (noncontact or remote measurements);
2) finite thickness of air which may be used for crack-detection optimization if its presence enhances crack detection;
3) finite thickness of a dielectric with dielectric properties equal to those of free-space (i.e., covered crack case).

Therefore, it is important to study the effect of lift-off on the *crack characteristic signals*. Fig. 6 shows the normalized calculated and measured *crack characteristic signals* recorded at a frequency of 24 GHz, for a crack with a width of 0.51 mm and a depth of 3 mm at flush (contact) and at a lift-off of 1 mm, respectively. Again, with a lift-off, the distance between the two sharp transitions in the *crack characteristic signal* increases (similar to covered cracks). Also, the level of the *crack characteristic signals* and their variations within the scanned distance reduce remarkably. This may be interpreted as the sensor (waveguide aperture) not being sensitive to the presence of the slot beyond a certain lift-off distance. However, it may be concluded that even at 1-mm lift-off there is still considerable variations in the overall shape of the *crack characteristic signal*. Therefore, the crack should still be detected at larger lift-offs. Clearly, the sensitivity of the detector diode plays a major role in detecting faint signal variations. This parameter may significantly influence the measurements.

The variations in the calculated *crack characteristic signals* compared to the measured ones in Figs. 5 and 6 are mainly attributed to the specific diode characteristics, a deviation from the actual value of the dielectric constant for the dielectric-coating layer as used in the calculations, the number of modes used due to the limited computer resources, as well

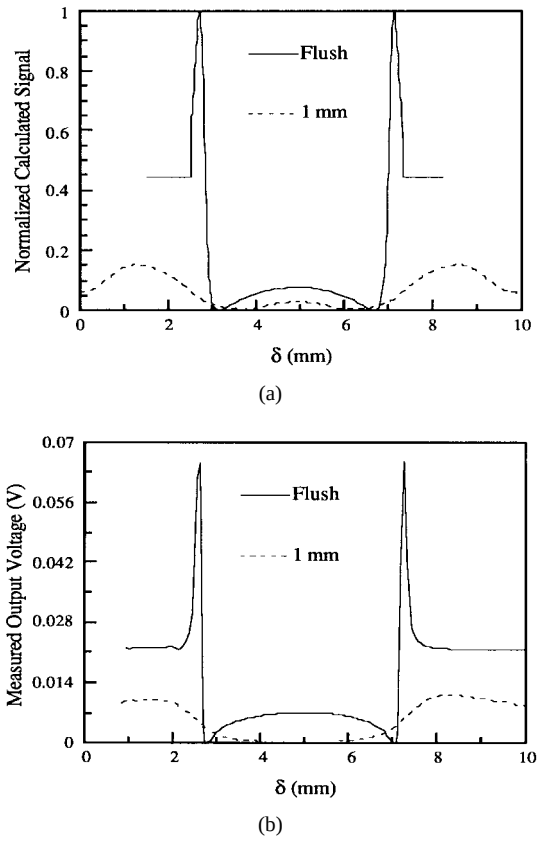

Fig. 6. Crack characteristic signals for a crack with a width of 0.51 mm and a depth of 3 mm at flush, and at a lift-off of 1 mm at a frequency of 24 GHz. (a) Calculated. (b) Measured.

as the assumption of a bounded dielectric-coating layer in the theoretical evaluations (i.e., a system of waveguides). This last effect was already shown in Section III-C when studying this assumption, and results were compared with the infinite half-space (Table I).

VIII. Conclusions

This moment-solution approach has proven to be a powerful technique for theoretically evaluating *crack characteristic signals* for covered cracks. This *dynamic* (the location of the crack is continuously changing relative to the probing waveguide aperture) electromagnetic model is versatile and allows us to evaluate empty and filled cracks covered with a dielectric-coating layer or with a standoff distance. The validity of the representation of a dielectric-coating layer as a waveguide section is tested. A convergence plane is calculated in order to evaluate an appropriate number of basis functions for the two junctions and an appropriate number of modes in the dielectric-coating layer for convergence. This model may be used to optimizing measurement parameters for increased detection sensitivity.

This microwave approach is shown to be capable of detecting surface cracks under dielectric coatings such as paint, corrosion preventative coatings, etc. It is shown that cracks under coatings of 1 mm are detected. Thin dielectric-coating layers ($\approx<$0.1-mm thick) may improve crack detection in two ways. The sharp transition becomes gradual (i.e., no need for high resolution scanners), and also in some cases there is an improvement in the dynamic range of the detected signal (if the location of the detector diode is fixed). Thus, in practice, a thin layer of dielectric may be introduced between the waveguide aperture and the specimen surface to improve detection sensitivity, particularly for fixed diode positions.

References

[1] K. G. Boving, *NDE Handbook, Non-Destructive Examination Methods for Condition Monitoring*. Denmark: Teknisk Forlag A/S, 1989.
[2] C. Yeh and R. Zoughi, "A novel microwave method for detection of long surface cracks in metals," *IEEE Trans. Instrum. Meas.*, vol. 43, pp. 719–725, Oct. 1994.
[3] C. Yeh, E. Ranu, and R. Zoughi, "A novel microwave method for surface crack detection using higher order waveguide modes," *Mat. Eval.*, vol. 52, no. 6, pp. 676–681, June 1994.
[4] C. Yeh and R. Zoughi, "Sizing technique for surface cracks in metals," *Mat. Eval.*, vol. 53, no. 4, pp. 496–501, Apr. 1995.
[5] ——, "Microwave detection of finite surface cracks in metals using rectangular waveguide sensors," *Res. Nondestructive Eval.*, vol. 6, no. 1, pp. 35–55, 1994.
[6] S. Ganchev, R. Zoughi, C. Huber, R. Runser, and E. Ranu, "Microwave method for locating surface crack tips in metals," *Mat. Eval.*, vol. 54, no. 5, pp. 598–603, May 1996.
[7] R. Zoughi, S. I. Ganchev, C. Huber, E. Ranu, and R. Runser, "A novel microwave method for filled and covered surface crack detection in steel bridge members including crack tip identification," Federal Highway Administration, McLean, VA, 4th Annual Rep. Contract DTFH61-94-X-00023, Sept. 1995.
[8] R. F. Harrington, *Time Harmonic Electromagnetic Fields*. New York: McGraw-Hill, 1961.
[9] ——, *Field Computation by Moment Methods*. New York: Krieger, 1982.
[10] R. F. Harrington and J. R. Mautz, "A generalized network formulation for aperture problems," *IEEE Trans. Antennas Propagat.*, vol. AP-24, pp. 870–873, Nov. 1976.
[11] F. E. Borgnis and C. H. Papas, *Encyclopedia of Physics: Electromagnetic Waveguides and Resonators*, vol. 16. Berlin, Germany: Springer-Verlag, 1958.
[12] N. Marcuvitz, *Waveguide Handbook*. New York: McGraw-Hill, 1951.
[13] J. Audet, J. Bolomey, C. Pichot, D. Nguen, M. Robillard, M. Chive, and Y. Leroy, "Electrical characteristics of waveguide applicators for medical applications," *J. Microwave Power*, vol. 15, pp. 177–186, Sept. 1980.
[14] L. Lewin, *Advanced Theory of Waveguides*. London, U.K.: Iliffe, 1951.
[15] S. I. Ganchev, S. Bakhtiari, and R. Zoughi, "A novel numerical technique for dielectric measurement of generally lossy dielectrics," *IEEE Trans. Instrum. Meas.*, vol. 41, pp. 361–365, June 1992.
[16] C. Huber, "Electromagnetic modeling of exposed and covered surface crack detection using open-ended waveguides," Ph.D. dissertation, Elect. Eng. Dept., Colorado State Univ., 1996.
[17] R. E. Collin, *Foundations for microwave engineering*, 2nd. ed. Piscataway, NJ: IEEE Press, 1992.

Christian Huber (M'96) received the Dipl.-Ing. degree in communications engineering from the Technical University of Vienna, Vienna, Austria, in 1992, and the Ph.D. degree in electrical engineering (microwave NDT and NDE) from Colorado State University, Ft. Collins, in 1995.

While with AMNTL, his research was on fatigue crack detection on exposed and covered metal surfaces using open-ended rectangular waveguides. He is currently with Anaren Microwave, Inc., Syracuse, NY. He is involved in the research and design of microwave integrated circuits (MMIC's) at $K\alpha$-band frequency range. These designs include antenna arrays, antenna feed networks, beam-forming networks, etc., for space and radar applications.

Dr. Huber is the recipient of the IEEE Microwave Theory and Techniques Society Graduate Fellowship Award in 1994. He has also been recognized as an honored researcher by the Colorado State University Research Foundation in 1994 and 1995, respectively.

H. Abiri, photograph and biography not available at time of publication.

Stoyan I. Ganchev (M'92–SM'92) received the M.Sc. degree in physics from the University of Sofia, Sofia, Bulgaria, in 1969, and the Ph.D. degree from the Institute of Electronics, Bulgarian Academy of Sciences, Bulgaria, in 1985.

From 1969 to 1990, he was engaged in research on microwave ferrites and ferrite devices at the Institute of Electronics. From 1990 to 1997, he served as the Senior Research Associate at the Applied Microwave Nondestructive Testing Laboratory, Department of Electrical Engineering, Colorado State University, Ft. Collins. He is currently with Hewlett-Packard Company, Englewood, Colorado. His research interest is in microwave nondestructive evaluation, and has extensively published in this area.

R. Zoughi (S'85–M'86–SM'93) received the B.S.E.E., M.S.E.E., and Ph.D. degrees in electrical engineering (radar remote sensing, radar systems, and microwaves) from the University of Kansas, Lawrence, in 1982, 1983, and 1987, respectively.

From 1981 to 1987, he was employed by the Radar Systems and Remote Sensing Laboratory (RSL), University of Kansas, in various capacities. His experience at RSL included developing, building, and operating various radar systems, data collection, and analysis. Since 1987, he has been with Colorado State University, Ft. Collins, where he is currently a Professor in the Electrical Engineering Department, where he established the Applied Microwave Nondestructive Testing Laboratory. He has published over 150 journal publications, conference presentations and proceedings, technical reports, and overview articles in the fields of radar remote sensing and microwave nondestructive evaluation. His current areas of research include NDT of material using microwaves, developing new techniques for microwave and millimeter-wave inspection and testing of materials, and developing new electromagnetic probes to measure characteristic properties of material at microwave frequencies.

Dr. Zoughi is a senior member of Sigma Xi, Eta Kappa Nu, and the American Society for Nondestructive Testing (ASNT). He has been voted the most outstanding teaching faculty for the past six years at Colorado State University. He is an associate technical editor for *Materials Evaluation* and has served as the guest associate editor for the special microwave NDE issue of *Research in Nondestructive Evaluation* in 1995. He has also been recognized as an honored researcher for the last four years by the Colorado State University Research Foundation. He is the recipient of the Dean's Council Award in 1992, and the Abell Faculty Teaching Award in 1995. He is also the Business Challenge Endowment Associate Professor of Electrical Engineering (1995–1997), and the 1996 recipient of the Colorado State Board of Agriculture Excellence in Undergraduate Teaching Award.